



## Supplementary Materials for

### **Amyloid $\beta$ oligomers constrict human capillaries in Alzheimer's disease via signaling to pericytes**

**Ross Nortley<sup>1</sup>, Nils Korte<sup>1\*</sup>, Pablo Izquierdo<sup>1\*</sup>, Chanawee Hirunpattarasilp<sup>1\*</sup>, Anusha Mishra<sup>2\*</sup>, Zane Jaunmuktane<sup>3,4\*</sup>, Vasiliki Kyrargyri<sup>1\*</sup>, Thomas Pfeiffer<sup>1</sup>, Lila Khennouf<sup>1</sup>, Christian Madry<sup>1</sup>, Hui Gong<sup>1</sup>, Angela Richard-Loendt<sup>4</sup>, Wenhui Huang<sup>5</sup>, Takashi Saito<sup>6</sup>, Takaomi C. Saido<sup>6</sup>, Sebastian Brandner<sup>3,7</sup>, Huma Sethi<sup>8</sup> and David Attwell<sup>1+</sup>**

\* These authors made an equal contribution

correspondence to: [d.attwell@ucl.ac.uk](mailto:d.attwell@ucl.ac.uk)

#### **This PDF file includes:**

Figure S1. Morphological identification of pericytes.

Figure S2. Circumferential processes of pericytes are mainly near the soma.

Figure S3. Constriction of capillaries by pericytes occurs predominantly at somata.

Figure S4. A $\beta$  depletes reduced glutathione (GSH) in pericytes and microglia.

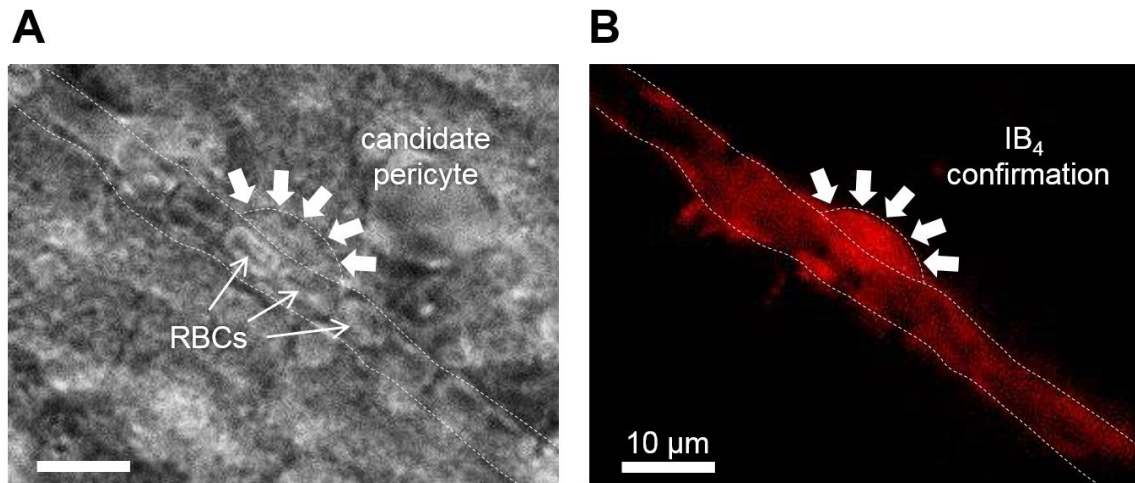
Figure S5. Amyloid plaques in different regions of AD mouse brain.

Figure S6. Endothelin-1 has different effects on capillaries and arterioles.

Figure S7. Oxygen levels are lower in the cortex of AD mice.

Figure S8. Pathways regulating pericyte contraction.

References (51-52).



**Fig. S1. Morphological identification of pericytes.**

(A) Bright field image showing a morphologically-identified candidate pericyte on a rat capillary, with the soma exhibiting the classical bump-on-a-log appearance. Pericytes were identified by the experimenter using images like this, without inspecting the IB<sub>4</sub> fluorescence. (B) Same field with IB<sub>4</sub>-Alexa-568 fluorescence excited, showing that the soma is surrounded by IB<sub>4</sub>-labeled basement membrane, and thus is confirmed to be a pericyte. In 26 out of 27 trials (96.3%), IB<sub>4</sub> fluorescence confirmed the morphologically selected cells to be pericytes.

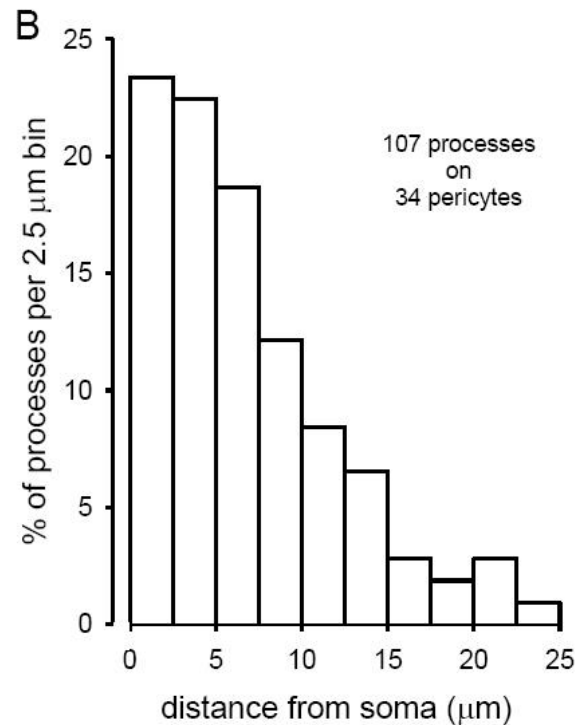
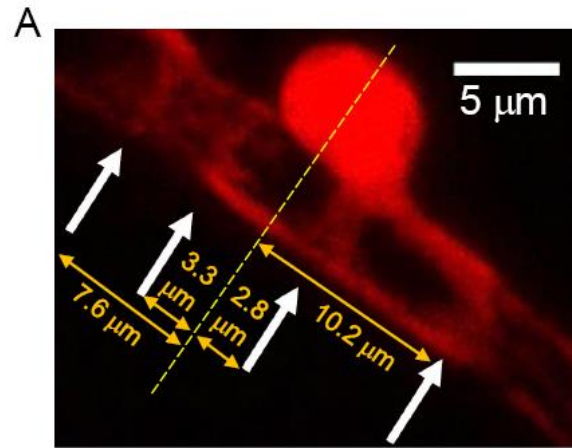


**Fig. S2. Circumferential processes of pericytes are mainly near the soma.**

(A) Confocal image (maximum intensity projection) of a mouse capillary pericyte transgenically labeled with dsRed under the NG2 promoter, showing circumferential processes at different distances from the soma. (B) Distribution of the percentage of circumferential processes (per 2.5 μm bin) as a function of distance along the capillary from the centre of the somata of 34 pericytes. To be defined as “circumferential”, and thus potentially able to reduce capillary diameter when contracted, a process had to run at  $>35^\circ$  to the axis of the capillary. Defined thus, 77% of circumferential processes were within 10 μm of the centre of the soma.

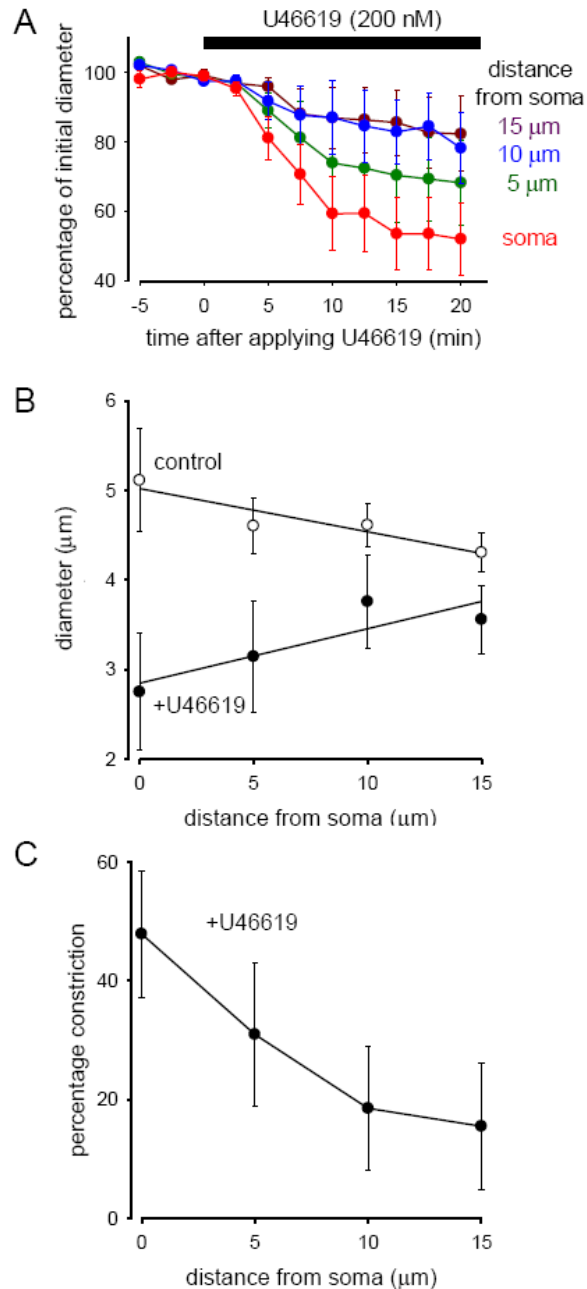


**Fig. S3. Constriction of capillaries by pericytes occurs predominantly at somata.** (A) Time course of capillary constriction at different distances from 5 rat pericytes on application of the thromboxane  $A_2$  analogue U46619 (200 nM). A greater constriction is produced near the somata. (B) Mean diameter as a function of distance from pericyte somata before U46619 was applied (control) and after 20 mins application (+U46619). Note larger mean diameter near the somata in the absence of vasoconstrictor, as is found in non-AD biopsy tissue from human subjects (Fig. 4D) and in vivo in non-AD mice (Fig. 5F). (C) Percentage constriction (from panel B) in U46619 as a function of distance from the somata shows that the constriction reflects the distribution of circumferential processes seen in Fig. S2.

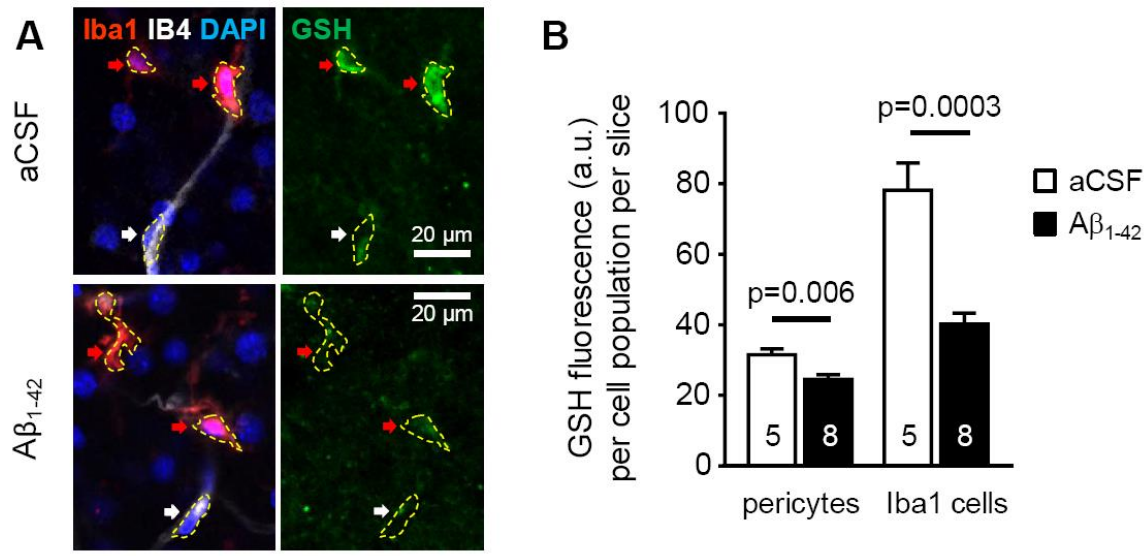


**Fig. S4.  $A\beta$  depletes reduced glutathione (GSH) in pericytes and microglia.**

(A) Representative images of microglia (red arrows) and pericytes (white arrows) labeled for GSH (right panels) in rat neocortical slices. Top panels: control conditions, when microglia show a higher level of GSH than pericytes (note that the pericyte nucleus does not label for GSH). Bottom panels: in the presence of 72 nM  $A\beta$ , which lowers the GSH level in both pericytes and microglia. Yellow dashed lines indicate measurement ROIs.

(B) Quantification of GSH level for the population of pericytes and microglia averaged across 3 images from each slice. Numbers on bars are of slices. Quantification per individual pericyte and microglial cell is given in the main text.

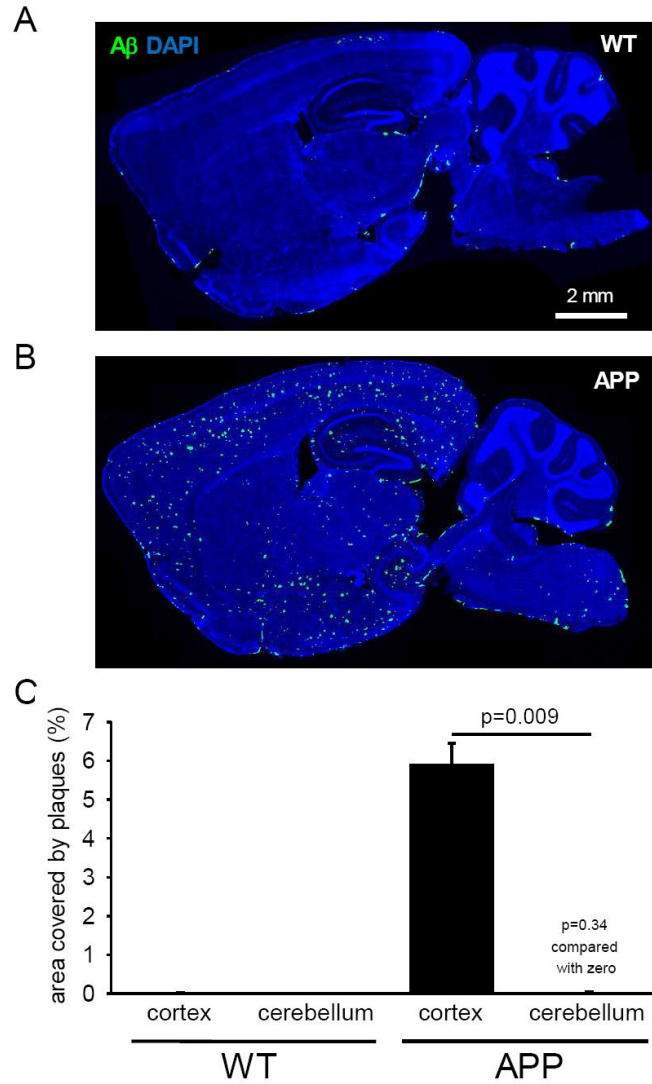


**Fig. S5. Amyloid plaques in different regions of AD mouse brain.**

(**A**, **B**) Wild-type (WT, **A**) and AD (APP, **B**) brains labeled with DAPI (blue) and for amyloid plaques with 82E1 antibody (green). Green areas at the edge of tissue regions are artefacts (resulting from the automated scanner for the image acquisition changing focus), and were excluded from the quantitative analysis (**C**) Quantification of fraction of area labeled for plaques in the neocortex and cerebellum of 2 WT and 3 AD mice.

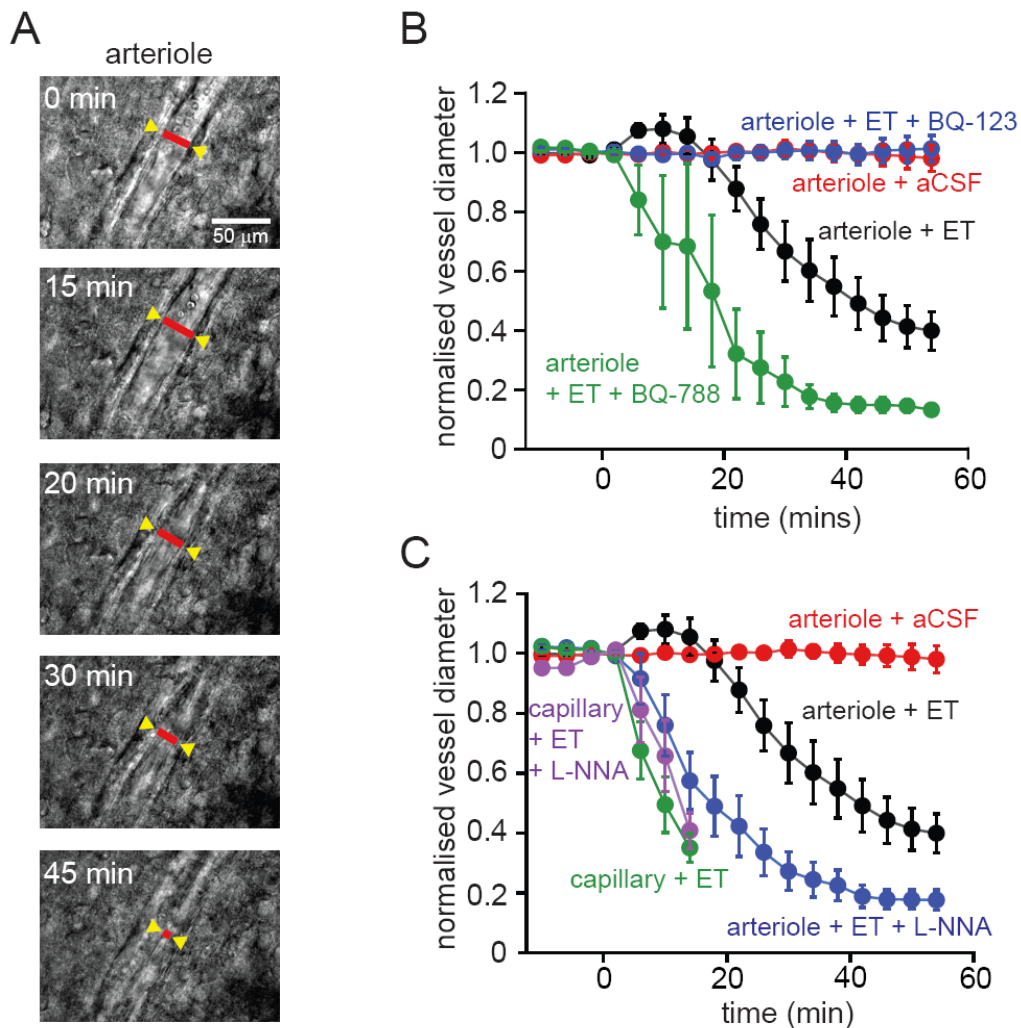


**Fig. S6. Endothelin-1 has different effects on capillaries and arterioles.**

(A) Images of a representative arteriole in a rat cortical brain slice showing its response to ET (10 nM), with an initial dilation, followed by a constriction. (B) Mean time course of biphasic response to ET (black dots, n=10 arterioles), which does not occur with aCSF (red, n=8). These diameter changes are abolished by the ET<sub>A</sub> blocker BQ-123 (blue, 1 nM, n=11). Blocking ET<sub>B</sub> receptors with BQ-788 (green, 1  $\mu$ M, n=6) abolishes the dilation and greatly speeds the constriction evoked by ET. (C) The constriction evoked by ET in arterioles (black, n=10) is much slower than that evoked in capillaries (green, n=10). Blocking NO synthase with L-NNA (1 mM) greatly speeds the constriction evoked by ET in arterioles (blue, n=12) but has little effect on the speed of the constriction in capillaries (purple, n=9). Plots show mean ( $\pm$ s.e.m) diameter of vessels (as

labeled). These experiments suggest a reason for the lack of a constriction of arterioles by endogenous A $\beta$  in the AD mice, as follows. Endothelin-1 evokes an initial dilation of arterioles followed by a constriction that was much slower than that seen for capillaries (panels A-C). Blocking ET<sub>B</sub> receptors or NOS converts this biphasic response into a constriction with a time course similar to that seen in capillaries (panels B-C). This is consistent with arteriolar smooth muscle contracting (like pericytes) when endothelin-1 activates ET<sub>A</sub> receptors on the contractile cells, but with the activation of ET<sub>B</sub> receptors linked to NOS (probably in endothelial cells or interneurons) evoking an opposing arteriole dilation. Presumably, at the levels of endogenous A $\beta$  and endothelin-1 reached in AD, the dilation and constriction approximately cancel out (as no diameter change was seen in arterioles in AD mice), whereas with application of exogenous A $\beta$  in previous work (12) the contraction dominated.



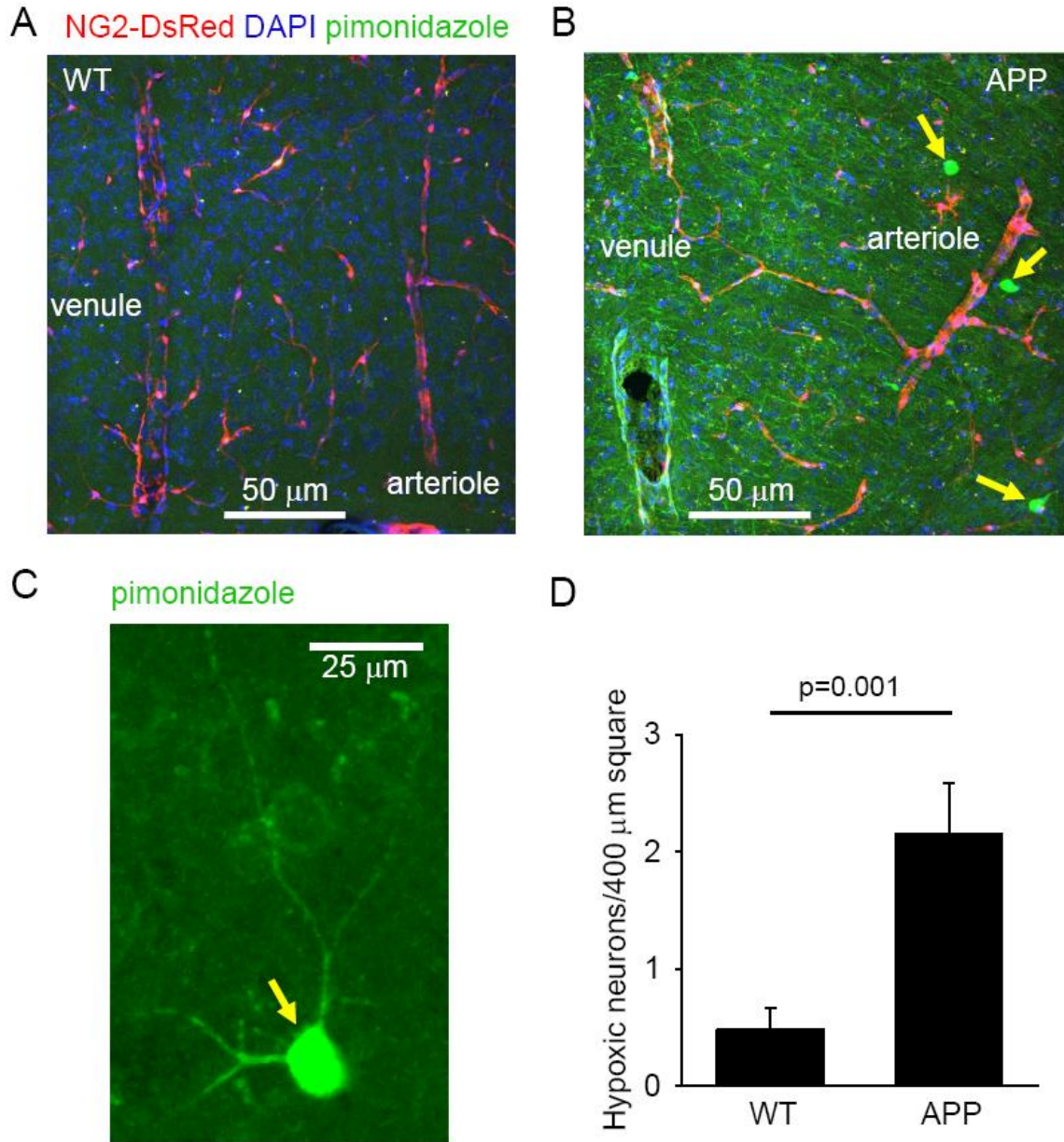


**Fig. S7. Oxygen levels are lower in the cortex of AD mice.**

(A-B) Representative images of sections of cortex from 4 month old WT (A) and AD (APP, B) mice, labeled with pimonidazole (green) and NG2-DsRed (red), showing more labeling in the AD mouse, where the labeling intensity was higher on the venous side of the vasculature (as seen previously (51)) and there was sparse bright labeling of hypoxic neurons (yellow arrows, these might be interneurons that are firing at a high rate (52), and thus may be more metabolically challenged, therefore showing larger hypoxia in the AD mice which have constricted capillaries). (C) Expanded view of a hypoxic neuron. (D) Quantification of number of hypoxic neurons (per 400 μm x 400 μm, x 10 μm deep stack) in AD (APP) and wild-type (WT) mice. In WT mice 21 stacks from 3 mice were examined, and in AD mice 26 stacks from 3 mice were examined.

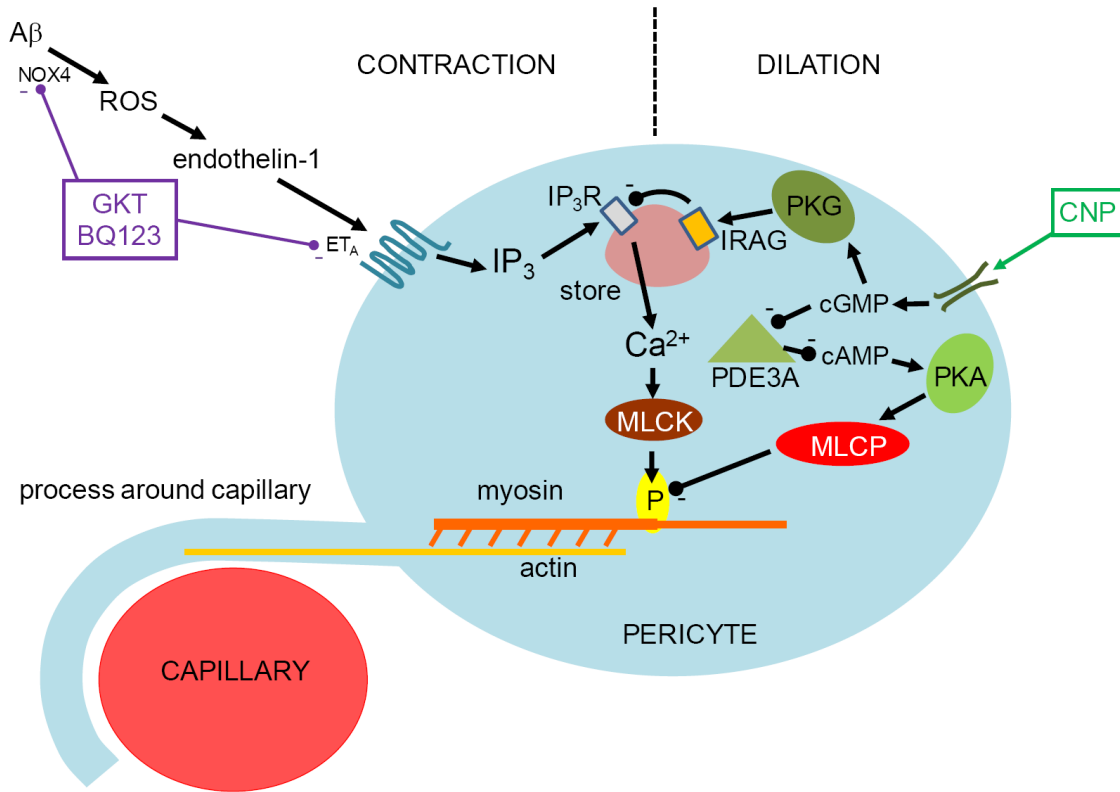


**Fig. S8. Pathways regulating pericyte contraction.**

Schematic diagram of a pericyte with a contractile process around a capillary. A $\beta$  generates ROS (via NOX4) which evoke release of endothelin-1 (ET), which can activate contraction by binding to ET<sub>A</sub> receptors. These generate IP<sub>3</sub> to release Ca<sup>2+</sup> from internal stores, which evokes contraction by activating myosin light chain kinase (MLCK). This pathway can be inhibited by blocking NOX4 with GKT137831 (GKT) and blocking ET<sub>A</sub> receptors with BQ-123. Alternatively, C-type natriuretic peptide (CNP) can block the ET-evoked contraction by acting on guanylate cyclase receptors that generate cGMP. This inhibits Ca<sup>2+</sup> release from stores by activating protein kinase G to phosphorylate the IP<sub>3</sub>R interacting protein IRAG. cGMP also inhibits cAMP phosphodiesterase 3A (PDE3A) leading to a rise of [cAMP] which activates protein kinase A (PKA) which in turn activates myosin light chain phosphatase (MLCP) to inhibit contraction.